

D. N. Sørensen

Research Scientist,
Department of Energy Engineering,
Technical University of Denmark,
DK2800 Lyngby, Denmark

M. C. Thompson

Research Scientist,
Department of Mechanical Engineering,
Monash University,
Clayton, Vic. 3168, Australia

J. N. Sørensen

Associate Professor,
Department of Energy Engineering,
Technical University of Denmark,
DK2800 Lyngby, Denmark

Toward Improved Rotor-Only Axial Fans—Part II: Design Optimization for Maximum Efficiency

Numerical design optimization of the aerodynamic performance of axial fans is carried out, maximizing the efficiency in a design interval of flow rates. Tip radius, number of blades, and angular velocity of the rotor are fixed, whereas the hub radius and spanwise distributions of chord length, stagger angle, and camber angle are varied to find the optimum rotor geometry. Constraints ensure a pressure rise above a specified target and an angle of attack on the blades below stall. The optimization scheme is used to investigate the dependence of maximum efficiency on the width of the design interval and on the hub radius. [S0098-2202(00)01602-3]

1 Introduction

Fan engineers are frequently faced with the problem of designing high-efficiency fans at a given flow rate and for a given pressure duty. Design techniques are typically based on engineering experience, and may involve much trial and error before an acceptable design is found. Calculating the specific rotational speed and diameter, discussed by e.g., Wright [1], may aid the designer in determining reasonable values for the rotational speed and diameter of the rotor, based on desired flow rate and pressure rise. Integrating the concept of free vortex flow design (Wallis [2]) in the process reduces the need to build and evaluate new designs. However, the restrictions of the spanwise distributions of velocity and pressure in the free vortex flow design imply that analysis of the fan at off-design duties has only limited validity.

In the work by Wallis [3], an inlet guide vane-rotor-stator installation was investigated. The system considered was of the free vortex flow type and several important parameters, e.g., lift-to-drag ratio, were fixed at reasonable values. This resulted in explicit expressions for efficiency and total pressure rise as a function of tip speed ratio, hub-to-tip ratio, and downstream losses. Parametrical studies of efficiency and pressure rise as a function of the three variables were then carried out.

Recently, Dugao et al. [4] considered numerical design optimization of a rotor-stator configuration for mining ventilation. Employing a free vortex flow design method, considerable improvement in efficiency was gained as compared to an existing installation. Furthermore, as an additional advantage, it was found that the noise emission from the fan installation was reduced.

The above investigations concerned fan performance for a fixed flow rate and pressure rise, i.e., at a predefined design point. Operating the fan under other conditions was not considered and it is therefore possible that it may behave poorly away from the design point. In practice, fans often operate far from the design point and often with low efficiency (Bolton [5]).

Employing an arbitrary vortex flow model (Sørensen and Sørensen [6]) for fan analysis enables the designer to investigate a fan operating under various conditions. Furthermore, a wide range of design alternatives may be tested numerically with equal validity. However, the increased degree of freedom of the arbitrary vortex flow model implies a trial and error process before an

acceptable design is found. This in turn limits the number of design variations that may be investigated as well as the complexity of the geometric requirements and operating conditions for the fan.

Design optimization techniques may be used to automate the fan design process. Here, searching algorithms maximize the efficiency while enforcing constraints on geometry, operating conditions and operating limits. Design parameters are automatically varied by the optimization algorithm and the corresponding changes in efficiency and constraints are used to determine an optimal design. Combining an optimization algorithm with the arbitrary vortex flow model enables the fan designer to investigate a large range of design alternatives in an efficient manner. Furthermore, parametrical studies of optimum designs for various operating conditions and geometrical requirements are easily carried out. Many fan configurations are compared in the optimization algorithm and a computationally efficient implementation of the arbitrary vortex flow model is required. In Sørensen and Sørensen [6], a Newton-Raphson method was used to solve the equations of the model, and solutions converged to machine accuracy are found at small computing costs. Furthermore, results agree well with measurements and this model is therefore used in the present work.

The efficiency of a rotor-only fan is considered over a design interval of flow rates rather than at a design point. This enables the design of a fan that operates well under various conditions. The fan duty and size are determined from the specific application of the fan. In the present case, the basis used for the optimizations is the fan from Kahane [7], which was also used for validating the aerodynamic model in Sørensen and Sørensen [6].

In Section 2, a description of the mathematical optimization problem, as applied to fan efficiency maximization, is given. Furthermore, some special implementation details of the optimization algorithm are discussed. In Section 3, optimizations are carried out to clarify the dependence of the efficiency on the width of the design interval and on the hub radius of the rotor.

2 Method

The standard constrained optimization problem can be formally stated as

$$\begin{aligned} &\text{Maximize } F(\Phi_n) && n = 1, 2, \dots, \text{NDV} \\ &\text{subject to } g_j(\Phi_n) \geq 0 && j = 1, 2, \dots, \text{NCON}, \end{aligned}$$

Contributed by the Fluids Engineering Division for publication in the JOURNAL OF FLUIDS ENGINEERING. Manuscript received by the Fluids Engineering Division October 21, 1997; revised manuscript received January 21, 2000. Associate Technical Editor: B. Schiavello.

where NDV denotes the number of design variables and NCON the number of constraints.

The objective function, F , describes the fitness of the possible designs and, in the present case, reflects the requirements of the manufacturer to produce a high-efficiency fan. The design variables, denoted by Φ_n , define the possible configurations, which can be altered by the optimization algorithm so as to find the maximum of F . Finally, g_j denotes the constraints which describe geometrical restrictions of the designs as well as desired operating conditions and limits of the fan.

In Section 2.1, the definition of the objective function in terms of maximum efficiency is described. The design variables governing the optimization problem are defined in Section 2.2. The constraints, imposing practical restrictions to blade geometry and operating conditions, are discussed in Section 2.3. Finally, in Section 2.4 a brief description of the implementation of the optimization algorithm is provided.

2.1 The Objective Function. Defining a design interval of flow rates and denoting the center of the design interval by Q_c and width by ΔQ , respectively, the primary goal of the optimization is to maximize the mean value, $\bar{\eta}$, of the aerodynamic fan efficiency in the design interval, $Q \in [Q_c - 1/2\Delta Q; Q_c + 1/2\Delta Q]$ [m^3/s].

The mean value is defined by

$$\bar{\eta} = \frac{1}{\Delta Q} \int_{Q_c - 1/2\Delta Q}^{Q_c + 1/2\Delta Q} \eta(Q) dQ, \quad (1)$$

where the efficiency of the fan at a given flow rate, $\eta = \eta(Q)$, is calculated using the model described in Sørensen and Sørensen [6]. In the present work, $\eta(Q)$ is defined as

$$\eta = Q \cdot (p_T - \Delta p_D) / P, \quad (2)$$

where Q is the flow rate, $p_T = p_T(Q)$ is the total pressure rise across the fan rotor, $\Delta p_D = \Delta p_D(Q)$ is the loss in the downstream diffuser, and $P = P(Q)$ is the power input to the fluid. Besides the loss in the downstream diffuser, empirical correlations are used for the loss due to the tip clearance height and for the secondary drag losses. The above empirical loss correlations are further described in Sørensen and Sørensen [6]. Losses in seals, bearings, etc. are excluded from the optimization.

The total pressure rise, p_T , across the rotor is determined as a spanwise integration of the total pressure rise across each streamtube. Similarly, the input power is determined by an integration of the lift and drag contributions. For the rotor-only configuration considered here, the dynamic pressure contained in the tangential velocity cannot be regained and is not included in the calculation of p_T . In the following, the result from the optimization, i.e., the optimum (maximum) value of $\bar{\eta}$, is denoted $\bar{\eta}_{\max}$.

To evaluate the integral in Eq. (1), the design interval is divided into N_d equally spaced flow rate evaluation-points and the efficiency, η , is calculated at each of these points. The mean value, $\bar{\eta}$, is then calculated using an accurate numerical integration method of order $O(1/N_d^4)$ from Press et al. [8]. The integral is constructed by fitting cubic polynomials through successive groups of four points.

2.2 Design Variables. The chosen design variables, which define the various possible fan configurations, are the hub radius of the rotor, r_h , and the spanwise distributions of chord-length, $c(r)$, stagger-angle, $\xi(r)$, from the rotational axis and camber angle, $\theta(r)$, of the airfoils (Fig. 1). Although tip radius and angular velocity of the rotor are key design parameters, they are excluded in the present study. The rationale behind this is to show that, even though the optimized fans have the same dimensionless characteristics in terms of e.g., specific speed, differences in performance can be achieved, depending on the allowed variations in geometry and on the imposed limits on operating conditions.

The spanwise distributions of chord, stagger, and camber are defined using single segment Bézier curves. The radial positions

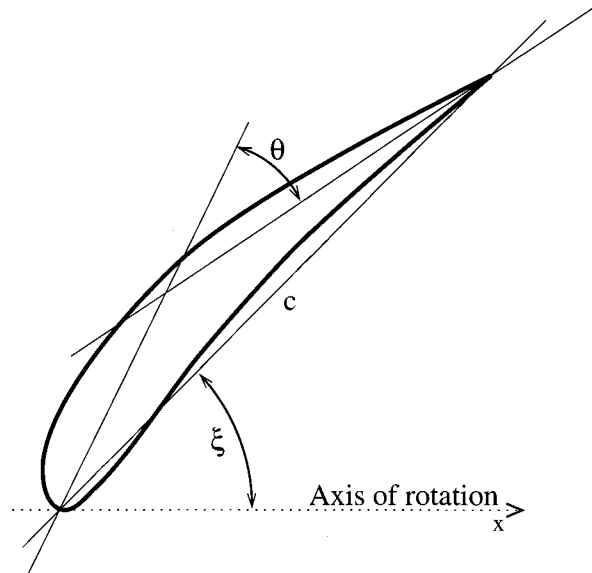


Fig. 1 Definition of the spanwise variables chord (c), stagger (ξ), and camber (θ), used in the optimization

of the vertices in the Bézier polygon are fixed and distributed evenly from hub to tip, whereas the lateral movement of the vertices defines the spanwise distribution of chord, stagger and camber. Thus, the number of design variables describing either of the spanwise distributions corresponds to the number of vertices in the Bézier polygon. An investigation of the required number of vertices in the Bézier polygon is carried out in Section 3.1.

The NACA65 airfoil family is used for the blades and measured airfoil cascade data are obtained from Emery et al. [9]. Only data for camber angles of 12 and 18 degrees were extracted, since these were measured using the broadest range of geometrical variations. The optimization algorithm requires differential functions and it was necessary to smooth the data. This was performed by creating explicit expressions for the lift and drag coefficients as a function of angle of attack, stagger angle, solidity, and camber angle. To find the functional expression which approximated the measurements best, using a least square measure, an unconstrained optimization problem was defined and solved numerically. To evaluate the quality of the functional expressions, the test case from Kahane [7], used in Sørensen and Sørensen [6] was recalculated using the functional expressions and it was found that the efficiency deviated less than 0.6 percent from the original calculations, for all of the investigated flow rates.

2.3 Constraints. Requirements from the manufacturer determine the specifications of the fan and thereby also the constraints. These may be due either to some geometrical restrictions or to some desired property of the fan as discussed below. In the present case, we consider a situation in which the fan used for validation in Sørensen and Sørensen [6] is to be improved, using the following specifications:

- The tip radius of the fan is fixed at $r_t = 0.27$ m.
- $B = 24$ blades is used for the rotor.
- The angular velocity is fixed at $\Omega = 3000$ rpm.
- The center of the design interval is defined as $Q_c = 6.0$ m^3/s . This value is chosen since the rotor providing the basis for the optimizations exhibits maximum efficiency at this flow rate when the definition of efficiency in Eq. (2) is used (Kahane [7]).
- The total pressure rise, as defined in Section 2.1, should be at least 1800 Pa. for all flow rates.
- The tip clearance height is taken to be constant, $t = 1$ mm and

the efficiency of the diffuser is taken to be $\eta_D=0.9$ or $\eta_D=0.95$. The coefficients for the secondary drag contribution are defined as $a=0.018$ and $b=0.02$.

For the spanwise distributions of chord, stagger, and camber, differentiable constraints are ensured by calculating the constraints from the parameterized Bézier curves rather than from the discrete points governing the streamtube centers. In the present work, the following constraints are imposed:

Hub Radius, r_h . Due to manufacturing requirements, r_h should be larger than 100 mm. Furthermore, the annulus between hub and tip is chosen to be larger than 30 mm. Thus $r_h - 0.1 > 0$ and $r_t - r_h - 0.03 > 0$. Here, r_t designates the tip radius of the rotor. These constraints are never active for the optimum designs.

Chord Distribution, c . Although not based on geometrical or structural considerations, the measured airfoil data are restricted to solidities between 0.5 and 1.5. To avoid extrapolations of the data, the chord is constrained to solidities between 0.52 and 1.48. Here, the solidity is defined as $\sigma = c/s$, where $s = 2\pi r/B$.

Stagger Distribution, ξ . No natural restrictions apply to the stagger angle and it is bounded between 2 and 88 degrees to aid the optimization algorithm in narrowing the possible values. Thus $[\xi(r) - 2]_{\min} > 0$ and $[88 - \xi(r)]_{\max} > 0$. These constraints are never active for the optimum designs.

Camber Distribution, θ . The measured airfoil data are restricted to camber angles between 12 and 18 degrees. To avoid extrapolations of the data, the camber angle is constrained to values between 12.1 and 17.9 degrees.

Total Pressure Rise, p_T . The designed fan must be able to produce at least the required total pressure rise for all flow rates in the design interval. In the present work, $p_T = 1800$ Pa. was chosen as the minimum pressure rise. Thus $[p_T(Q) - 1800]_{\min} > 0$.

Axial Velocity in Outlet. As discussed in Sørensen and Sørensen [6], the analysis model is unreliable if very small outlet velocities are found. A constraint is imposed, ensuring that, for all blade elements, the optimum design does not result in outlet velocities less than 0.26 of the inlet velocity at any flow rate in the design interval. This constraint is never active for the optimum designs.

Tangential Velocity in Outlet. The ratio of tangential to axial velocity at the outlet is kept below 1.1 for all streamtubes and for all flow rates. This limit is imposed to avoid vortex breakdown downstream of the rotor, a flow-state which cannot be captured by the aerodynamic model. The above criterion for vortex breakdown is based on Squire [10], where stability analysis was applied to three cases of uniform axial velocity with different spanwise distributions of tangential velocity. The analysis indicated that vortex breakdown occurs when the ratio of tangential to axial velocity is between 1.0 and 1.2, thus justifying the choice of 1.1 as the limit.

Stall Limit, $\Delta\alpha_{\text{stall}}$. At high angles of attack, the flow on the blades may stall. This results in large unsteady forces acting on the blades, followed by fatigue problems. Furthermore, a large increase in noise emission occurs under stalled conditions (Sharland [11]). Here, we define stall to occur when the lift coefficient reaches its maximum value and the corresponding angle of attack is denoted by α_{stall} . For all flow rates and for each blade element, the difference between α_{stall} and the actual angle of attack, α , is determined. Denoting the smallest of these differences by $\Delta\alpha_{\text{stall}}$, a flow well below stall is ensured by demanding that $\Delta\alpha_{\text{stall}} \geq 1$, thus keeping the angle of attack, for all flow rates and for all blade elements, at least one degree below stall.

2.4 Optimization Algorithm. The optimization problem proposed in Sections 2.1–2.3 defines a differentiable and nonlinear objective function to be solved with a set of nonlinear con-

straints. The algorithm chosen for the solution of the problem is the sequential quadratic algorithm by Han [12], extended by Powell [13].

The algorithm requires gradients of the objective function and constraints with respect to the design variables. Explicit differentiation of the aerodynamic model is very complicated and the gradients are evaluated approximately, using finite differences. The computational effort for each iteration in the optimization algorithm is thus proportional to the number of design variables, NDV.

3 Results and Discussion

The following proposed guidelines apply for an optimum design and will be further discussed later:

- The pressure rise decreases with increasing flow rate. Therefore, the pressure rise constraint applies at the highest flow rate in the design interval. Furthermore, this constraint is expected to be active for all optimum designs, since an excessive pressure rise results in increased tangential velocities which, in the present investigation of a rotor-only fan, is considered as loss.
- The angle of attack on the blade increases with decreasing flow rate. Thus, if active, the stall limit constraint applies at the lowest flow rate in the design interval.
- The loss in the downstream diffuser, as well as the tip clearance loss, increases with increasing hub radius. Thus, it is anticipated that the hub radii will be small for the optimum designs, thereby lowering the losses. However, for small hub radii, the blade speed is low at the inner part of the rotor and the axial throughflow velocity is small due to the large annulus area. Both of these conditions result in low relative velocities and it becomes difficult to exchange the required momentum at the inner part of the blade. This in turn results in lowered axial velocities at the hub and the constraint on the tangential velocity may become active.
- The optimizations are carried out for an interval of flow rates, and thus for an interval of axial throughflow velocities. For small hub radii, the low blade velocity, combined with the variations in axial velocity, results in large variations of the angle of attack on the blade elements. Although influenced by all operating conditions and limits, an essential parameter for an optimum design is a lift-to-drag ratio close to maximum for all blade elements. The large angle of attack interval at the inner region of the blade implies that, in some parts of the flow rate interval, this part of the blade operates at angles of attack far away from maximum lift-to-drag ratio. Furthermore, large variations in angles of attack implies that the stall limit constraint may become active.

Before the optimization was applied to a real case, initial investigations were carried out as described in Section 3.1. First, the effect of varying the number of Bézier vertices for the curves describing the spanwise distribution of chord, stagger, and camber was examined. Second, the effect of varying the number of calculation points in the design interval was examined. After these preliminary investigations, a series of optimizations aimed at finding the optimum efficiency for various design conditions was carried out. This is described in Sections 3.2 and 3.3.

3.1 Initial Investigations. As discussed in Section 2.4, the number of calls to the performance analysis model in each iteration increases approximately linearly with the number of design variables. Furthermore, the number of iterations in the optimization algorithm tends to increase with increasing number of design variables. It is thus extremely important to keep the number of vertices in the Bézier polygons, describing chord, stagger and camber, to a minimum without sacrificing the freedom of the design too much. A series of optimizations was carried out, varying the number of vertices in the Bézier polygons. Using $N_d = 19$ points in a design interval defined by $Q_c = 6 \text{ m}^3/\text{s}$ and $\Delta Q = 2 \text{ m}^3/\text{s}$, it was found that five vertices in the Bézier polygons resulted in an optimum efficiency determined within approxi-

mately 0.01 percent of the efficiency obtained with eight vertices. This accuracy is adequate and five vertices in the Bézier polygons are used in all of the following optimizations.

Another important factor affecting the computational effort during the optimizations is the number of points, N_d , chosen to divide the design interval when evaluating the integral in Eq. (1). A linear dependence exists between the number of points and the calculation time. Using the same optimization case as described above, but varying N_d , it was found that for $N_d \geq 13$, the optimum efficiency was essentially independent of N_d . Thus $N_d = 13$ points are used in all of the subsequent calculations of $\bar{\eta}$.

3.2 Dependence on Design Interval Width. In order to clarify the dependence of optimum efficiency, $\bar{\eta}_{\max}$, on the width of the design interval, a series of optimizations was carried out for various values of ΔQ . The optimizations were carried out with $B = 24$ blades and the center of the design interval was $Q_c = 6 \text{ m}^3/\text{s}$ for all cases. In Fig. 2, $\bar{\eta}_{\max}$ is shown as a function of ΔQ . Also included in the figure are vertical lines indicating when the constraints become active. At design interval widths of $\Delta Q = 1.4 \text{ m}^3/\text{s}$ and above, the constraint for the stall limit is active and for $\Delta Q = 1.8 \text{ m}^3/\text{s}$ and above, the constraint limiting the tangential velocity is active.

As expected, the optimum efficiency decreases with increasing width of the design interval. For small values of ΔQ , the angles of attack experienced by the blade elements are close to the angle of attack at maximum lift-to-drag ratio. However, increasing the width of the design interval, the range of angles of attack experienced by the blade elements increases and, at least for some parts of the design interval, the lift-to-drag ratio is far from maximum.

For $\Delta Q \geq 1.4 \text{ m}^3/\text{s}$, the stall constraint becomes active which means that the increasing angle of attack interval can only be expanded towards lower angles of attack for some of the blade elements, thus limiting the design further. In Fig. 2, this can be observed as a slightly more decreasing $\bar{\eta}_{\max}$. For $\Delta Q \geq 1.8 \text{ m}^3/\text{s}$, the tangential velocity constraint becomes active as well, which is seen as an even faster decrease of $\bar{\eta}_{\max}$. For ΔQ larger than the values shown in Fig. 2, it was not possible to obtain a feasible design. For the largest flow rate interval resulting in a solution, the geometry of the rotor is determined completely by the constraints and thus independent of the objective function used.

An important thing to note from Fig. 2 is that an axial fan which operates well in a design interval of e.g., $\Delta Q = 1.4 \text{ m}^3/\text{s}$ has a decrease in $\bar{\eta}_{\max}$ of only about two points compared to the case

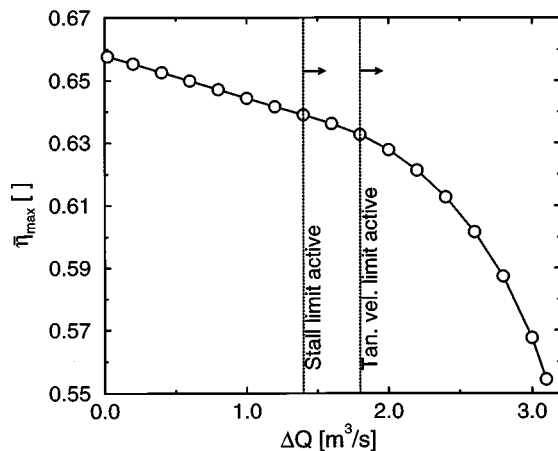


Fig. 2 Optimum efficiency as a function of design interval width, $Q_c = 6 \text{ m}^3/\text{s}$. The stall limit constraint is active for $\Delta Q \geq 1.4 \text{ m}^3/\text{s}$, and the tangential velocity limit constraint is active for $\Delta Q \geq 1.8 \text{ m}^3/\text{s}$.

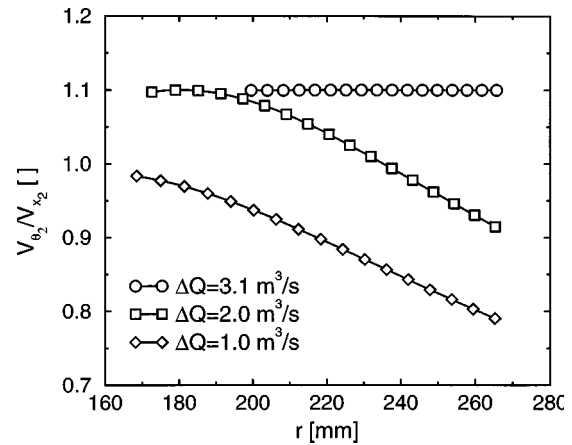


Fig. 3 Tangential to axial velocity ratio at fan outlet for the optimum designs for three different widths of the design interval. The curves are for the lowest flow rate in the design interval. The constraint on the tangential velocity was $V_{\theta_2}/V_{x_2} \leq 1.1$.

of $\Delta Q = 0 \text{ m}^3/\text{s}$. This indicates that axial fans which operate well under various conditions may be designed with the present method.

To further investigate the constraint on the tangential velocity, Fig. 3 shows the tangential to axial velocity ratio far downstream of the fan for three of the above design interval widths. All curves are for the lowest flow rate in the design interval ($Q = Q_c - \Delta Q/2$), at which the tangential to axial velocity ratio is maximum. It is seen that the tangential to axial velocity ratio constraint is not active for the case of $\Delta Q = 1.0 \text{ m}^3/\text{s}$. For $\Delta Q = 2.0 \text{ m}^3/\text{s}$ the constraint influences the inner part of the blade and for $\Delta Q = 3.1 \text{ m}^3/\text{s}$, the flow across the whole blade is determined by the constraint.

Figure 4 shows the optimum spanwise distributions of chord, stagger and camber, respectively, for the three design interval widths selected above. For $\Delta Q = 3.1 \text{ m}^3/\text{s}$, the case at which the tangential velocity constraint is active for all radii, the spanwise

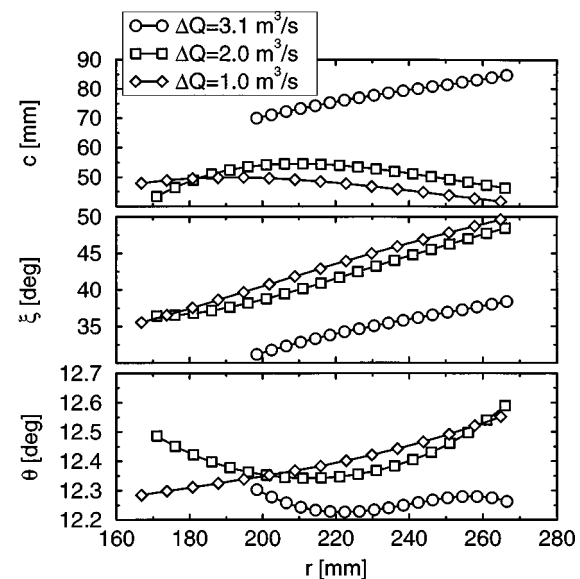


Fig. 4 Optimum spanwise distributions of chord (top), stagger angle (center), and camber angle (bottom) for three different widths of the design interval

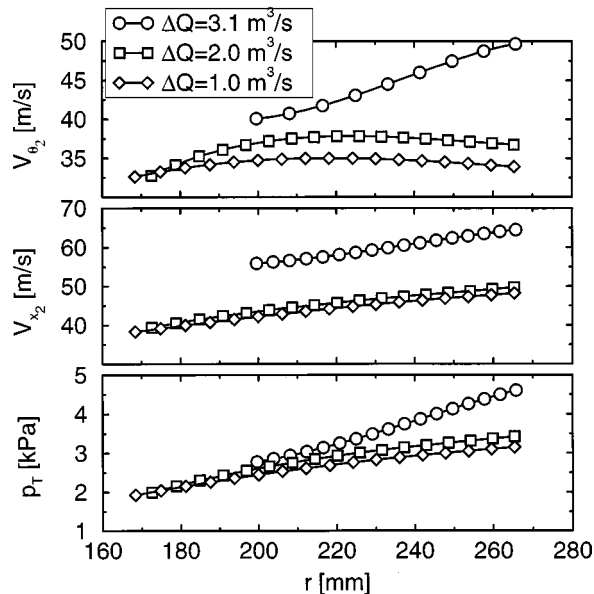


Fig. 5 Radial distributions of tangential velocity (top), axial velocity (center) and total pressure rise (bottom) for three different widths of the design interval. The curves are calculated at the flow rate of the design interval center ($Q_c = 6.0 \text{ m}^3/\text{s}$).

distributions are influenced by the constraint. This is most clearly seen on the chord distribution which increases nearly linearly from hub to tip. As noted above, this design interval is the largest at which a solution could be found and the design is determined by the constraints alone. For $\Delta Q = 2.0 \text{ m}^3/\text{s}$, the tangential velocity constraint is active at the inner part of the blade. This is reflected in the spanwise distributions with a significant increase in chord and an almost constant stagger angle at the inner part of the blade. Furthermore, the camber angle decreases at the inner part and increases at the outer part of the blade. Finally, for $\Delta Q = 1.0 \text{ m}^3/\text{s}$, where the constraints for the tangential velocity and for the stall limit both are inactive, the spanwise distributions exhibit a more regular behavior. Although a slight increase in chord is experienced at the inner part of the blade, the chord generally decreases toward the tip. The stagger angle and the camber angle increase all along the blade.

To further investigate the optimum designs, Fig. 5 depicts the spanwise distributions of tangential velocity, axial velocity, and total pressure rise, respectively, for the same three design interval widths as above. All curves are calculated at Q_c , the center of the design interval. For $\Delta Q = 3.1 \text{ m}^3/\text{s}$, the tangential velocity increases nearly linearly along the blade, with a relatively large gradient. This in turn results in a large variation in total pressure, increasing from the hub toward the tip. For $\Delta Q = 2.0 \text{ m}^3/\text{s}$, the geometry of the inner part of the blade is restricted due to the constraint on the tangential velocity. This is reflected in the tangential velocity distribution which increases significantly at the inner part of the blade after which it settles at a nearly constant value. For the spanwise distribution of total pressure rise, this is seen as a large increase at the inner part of the blade. Finally, for $\Delta Q = 1.0 \text{ m}^3/\text{s}$, the tangential velocity distribution increases slightly at the inner part of the blade, followed by a small decrease at the outer part of the blade. Generally, the tangential velocity is smaller than for the case with $\Delta Q = 2.0 \text{ m}^3/\text{s}$ which, for the distribution of total pressure rise, results in a smaller slope.

3.3 Dependence on Hub Radius. As discussed in the first part of Section 3, the losses in the downstream diffuser and from the tip clearance height increases with increasing hub radii. In the previous section, the hub radius was included as a design variable,

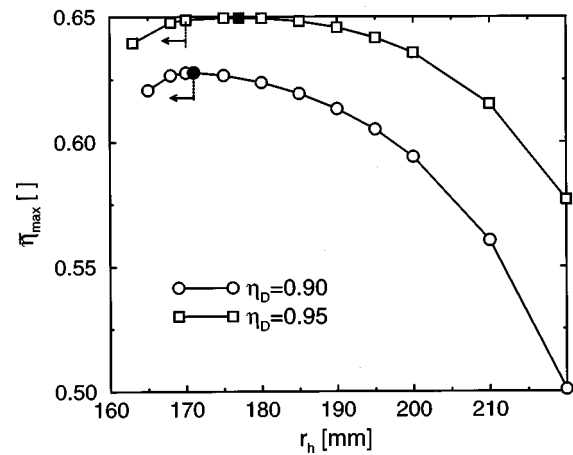


Fig. 6 Optimum efficiency as a function of hub radius. $Q_c = 6 \text{ m}^3/\text{s}$, $\Delta Q = 2 \text{ m}^3/\text{s}$. Filled symbols show the optimum hub radius, i.e., when the hub radius is included as a design variable. Arrows indicate when the tangential velocity limit constraint becomes active.

thereby obtaining the value which results in the highest efficiency of the fan. In this section, the sensitivity of the efficiency on the hub radius is investigated by carrying out a series of optimizations for varying hub radius, r_h . The center of the design interval is $Q_c = 6 \text{ m}^3/\text{s}$ and the width of the design interval is $\Delta Q = 2.0 \text{ m}^3/\text{s}$. As described in the introduction to Section 3, the downstream loss in the diffuser is highly influenced by the hub radius and the investigation is carried out using two different diffuser efficiencies, $\eta_D = 0.90$ and $\eta_D = 0.95$.

In Fig. 6 the efficiency as a function of hub radius is shown for the two diffuser efficiencies. Also included in the figure are the hub radii resulting in the optimum efficiency, determined by optimizations, where the hub radius was included as a design variable. These are indicated by solid symbols. The constraint for the stall limit was active for all optimizations and the constraint for the tangential velocity limit was active for small hub radii as indicated by arrows in the figure.

In accordance with the introductory remarks of Section 3, the optimizations with the larger downstream loss ($\eta_D = 0.90$) has a rapid decrease in optimum efficiency with increasing hub radius, whereas the case with a smaller downstream loss has a slower decrease. Also, the optimum hub radius marked with solid symbols, is larger for the case with the smaller downstream loss.

For small hub radii it becomes difficult to obtain the required pressure rise, thus limiting the geometry of the blades. This in turn results in a decreased efficiency, even though the downstream losses become smaller. For smaller hub radii than the ones shown in Fig. 6, it was not possible to obtain a solution to the optimization problem.

If the hub radius is determined from factors other than maximum efficiency, e.g., size of electrical motor or the use of standard hub designs, Fig. 6 may be used to investigate the consequences of the performance of the fan on changing the hub radius. As an example, it is seen that for the case of $\eta_D = 0.95$, the hub radius can be increased with approximately 25 mm from the optimum value with a decrease in efficiency of about two points. For the case of $\eta_D = 0.90$, the same efficiency decrease occurs for an increase in hub radius of about 22 mm.

4 Conclusion

An arbitrary vortex flow model for rotor-only axial fans has been combined successfully with a standard method for numerical design optimization of constrained nonlinear problems.

Optimizations were carried out to maximize the efficiency in a flow rate interval. The pressure rise was constrained to be above a required value at the high flow rate. Furthermore, the angle of attack was constrained to stay below stall at the low flow rate. To avoid vortex breakdown, a constraint was introduced, limiting the ratio of tangential to axial velocity in the outlet.

The dependence of optimum efficiency on the design interval width was investigated. For small design intervals, the efficiency is only weakly dependent on the design interval. Thus, fans that operate well for a range of flow rates may be designed using the present numerical optimization method, with only a limited penalty on efficiency.

The optimum efficiency was found to be dependent on hub radius. For very low hub radii, it is difficult to satisfy the imposed constraints and for large hub radii, losses due to tip clearance and due to the downstream diffuser becomes large. From this investigation, the implications of prescribing a certain hub radius can be estimated.

Finally, it must be emphasized that the objective function, design variables and constraints investigated in the present work are merely examples. The design method is quite general and can easily be extended to include other constraints and other design variables, or even a change of objective function.

Acknowledgments

The work was partly supported by the Danish Energy Agency under contract no. 1253/96-0002.

Nomenclature

a, b	= secondary drag coefficients
B	= number of blades
c	= chord length
F	= objective function (figure of merit)
g_j	= constraint no. j
NCON	= no. of constraints
NDV	= no. of design variables
N_d	= no. of design interval divisions
p_T	= integrated rotor pressure rise
Δp_D	= downstream diffuser loss
P	= mechanical shaft power
Q	= flow rate
Q_c	= flow rate at center of design interval
ΔQ	= width of design interval
r_h, r_t	= rotor hub and tip radii
s	= interblade spacing, $s = 2\pi r/B$

t	= tip clearance height
α	= angle of attack
α_{stall}	= angle of attack at stall
$\Delta\alpha_{\text{stall}}$	= minimum of all $\alpha_{\text{stall}} - \alpha$ values
η	= fan efficiency, $\eta = Q \cdot p_T / P$
$\bar{\eta}$	= mean value of fan efficiency in design interval
$\bar{\eta}_{\text{max}}$	= optimum fan efficiency
η_D	= downstream diffuser efficiency
Ω	= angular velocity of rotor
Φ_n	= design variable no. n
σ	= solidity, $\sigma = c/s$
θ	= camber angle
ξ	= stagger angle

References

- [1] Wright, T., 1996, "Low Pressure Axial Fans," *Handbook of Fluid Dynamics and Fluid Machinery. - 3: Applications of Fluid Dynamics*, J. A. Schetz and A. E. Fuhs, eds., Wiley, Chichester, pp. 2340–2356.
- [2] Wallis, R. A., 1961, *Axial Flow Fans. Design and Practice*, George Newnes Limited, London.
- [3] Wallis, R. A., 1968, "Optimisation of Axial Flow Fan Design," *Mechanical and Chemical Engineering Transactions, The Institution of Engineers, Australia*, **MC4**, No. 1, pp. 31–37.
- [4] Dugao, Z., Jiang, Z., and Song, J., 1996, "Optimization Design of an Axial Flow-Fan Used for Mining Local-Ventilation," *Comput. Ind. Eng.*, **31**, No. 3, pp. 691–696.
- [5] Bolton, A. N., 1990, "Installation Effects in Fan Systems," *Proceedings of the Institution of Mechanical Engineers, Part A 204*, pp. 201–215.
- [6] Sørensen, D. N., and Sørensen, J. N., 2000, "Toward Improved Rotor-Only Axial Fans—Part I: A Numerically Efficient Aerodynamic Model for Arbitrary Vortex Flow," *ASME J. Fluids Eng.*, **122**, No. 2, pp. 318–323.
- [7] Kahane, A., 1948, "Investigation of Axial-Flow Fan and Compressor Rotors Designed for Three-Dimensional Flow," *Tech. Note 1652*, NACA, Langley Memorial Aeronautical Laboratory, Langley Field, Va.
- [8] Press, W. H., Teukolsky, S. A., Vetterling, W. T., and Flannery, B. P., 1992, *Numerical Recipes in FORTRAN: The Art of Scientific Computing*, 2nd ed., Cambridge University Press, p. 128.
- [9] Emery, J. C., Herrig, L. J., Erwin, J. R., and Felix, A. R., 1958, "Systematic Two-Dimensional Cascade Tests of NACA 65-Series Compressor Blades at Low Speeds," Report TR-1368, NACA, Langley Aeronautical Laboratory, Langley Field, Va.
- [10] Squire, H. B., 1960, "Analysis of the vortex breakdown phenomenon. Part I," Report 102, Imperial College of Science and Technology, Aeronautics Department.
- [11] Sharland, I. J., 1964, "Sources of Noise in Axial Flow Fans," *J. Sound Vib.*, **1**, No. 3, pp. 302–322.
- [12] Han, S. P., 1976, "Superlinearly Convergent Variable Metric Algorithms for General Nonlinear Programming Problems," *Math. Program.*, **11**, pp. 263–282.
- [13] Powell, M. J. D., 1978, "A Fast Algorithm for Nonlinearly Constrained Optimization Calculations," *Lecture Notes in Mathematics*, G. A. Watson, ed., Vol. 630, pp. 144–157.